Quaternary Science Advances 12 (2023) 100110

Contents lists available at ScienceDirect

Quaternary Science Advances

journal homepage: www.sciencedirect.com/journal/quaternary-science-advances

Linking upwelling intensity and orbital-scale climate variability in South Africa's winter rainfall zone: Insights from a ~70,000-year hyrax midden record

Brian M. Chase [a,b,*], Andrew S. Carr [c], Arnoud Boom [c], Genevieve Tyrrell [c], Paula J. Reimer [d]

[a] Institut des Sciences de L'Evolution-Montpellier (ISEM), University of Montpellier, Centre National de La Recherche Scientifique (CNRS), EPHE, IRD, Montpellier, France
[b] Department of Environmental and Geographical Science, University of Cape Town, South Lane, Upper Campus, 7701, Rondebosch, South Africa
[c] School of Geography, Geology and the Environment, University of Leicester, Leicester, LE1 7RH, UK
[d] School of Natural and Built Environment, Geography, Archaeology and Palaeoecology, Queen's University Belfast, Belfast, BT7 1NN, Northern Ireland, UK

ARTICLE INFO

Keywords:
Late Quaternary
Benguela upwelling
Rainfall seasonality
Palaeoclimate
Rock hyrax middens
Stable isotopes

ABSTRACT

The climate of Africa's southwestern Cape is characterised by a strongly seasonal winter precipitation regime, with late Quaternary climate variability generally considered to have been driven by the position of the southern westerlies. This paper presents a unique ~70,000 year-long palaeoclimatic record from a rock hyrax midden from South Africa's winter rainfall zone, enabling the analysis of regional climate systems since the beginning of marine isotope stage 4. The data suggest that the last glacial period was relatively humid compared to the Holocene, likely due to cooler temperatures, more extensive Antarctic sea-ice extent and an equatorward displacement of the westerly storm track. However, orbital-scale climate variability associated with the 23 kyr precessional cycle primarily correlates with changes in upwelling intensity in the Benguela system, implying an important role for the blocking of tropical easterly flow in driving long-term climatic variability. These factors combined during glacial periods to significantly amplify rainfall seasonality in the southwestern Cape, bringing more winter rainfall via mid-latitude frontal systems, while reducing the proportion of summer rainfall, particularly during the glacial periods of the late Quaternary. The results therefore highlight the need to consider a complex suite of circulation systems and dynamics when inferring drivers of long-term environmental change in the region.

1. Introduction

The climate and environments of Africa's southwestern Cape differ markedly from the rest of southern Africa. Most of the subcontinent experiences a summer rain regime, determined by tropical convection potential and the transport of moisture from the southwest Indian Ocean and Agulhas region in the east (Crétat et al., 2012; Rouault et al., 2002; Tyson et al., 2002), and by the tropical Atlantic in the northwest (Crétat et al., 2019; Rouault et al., 2003). In contrast, the southwestern Cape receives most of its precipitation during the winter austral months via the extratropical westerlies and associated midlatitude frontal systems (Reason et al., 2002).

This spatial division in rainfall seasonality has led to the convention of dividing southern Africa into three rainfall regimes, the winter, summer and intermediate aseasonal or year-round rainfall zones (WRZ, SRZ and YRZ/ARZ respectively) (Chase and Meadows, 2007; Deacon and Lancaster, 1988; van Zinderen Bakker, 1976) (Fig. 1). This framework serves to simplify the diverse factors that determine rainfall variability across this region. Considering the responses of these zones to orbital forcing and late Quaternary glacial-interglacial cycles, early models of palaeoclimatic change in southern Africa hypothesised a coeval inverse response between the winter and summer rainfall zones (Cockcroft et al., 1987). Within such models, glacial periods were characterised by drier conditions in the summer rainfall zone as a result of lower sea-surface temperatures and reduced convection over the continent, while in the winter rainfall zone wetter conditions occurred due to the expansion of Antarctic sea ice and the equatorward displacement of the Subtropical Front and southern westerlies (Bard and

* Corresponding author. Institut des Sciences de L'Evolution-Montpellier (ISEM), University of Montpellier, Centre National de La Recherche Scientifique (CNRS), EPHE, IRD, Montpellier, France.
E-mail address: Brian.Chase@umontpellier.fr (B.M. Chase).

https://doi.org/10.1016/j.qsa.2023.100110
Received 14 June 2023; Received in revised form 28 July 2023; Accepted 28 July 2023
Available online 5 August 2023

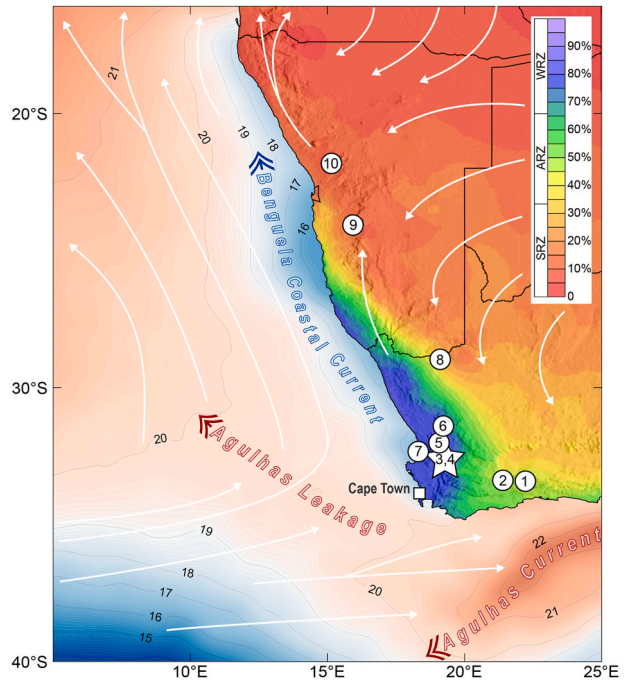

Fig. 1. Map of the southwestern margin of Africa showing seasonality of rainfall and sharp climatic gradients dictated by the zones of summer/tropical (red) and winter/temperate (blue) rainfall dominance. Winter, summer and aseasonal rainfall zones (WRZ, SRZ and ARZ respectively, defined according to Chase and Meadows (2007)). The major oceanic circulation systems (the cold Benguela current and the warm Agulhas and Angola currents, temperatures shown in °C (data from Reynolds et al., 2007)) and atmospheric circulation systems (white arrows) are indicated. The Groenfontein hyrax midden site (4, white star) is shown in relation to key palaeoclimatic records (1 – Cango Caves (Chase et al., 2021; Talma and Vogel, 1992) and Efflux Cave (Braun et al., 2020), 2 – Seweweekspoort (Chase et al., 2013, 2017), 3- Katbakkies Pass (Chase et al., 2015b; Meadows et al., 2010), 5 – De Rif (Chase et al., 2011, 2015a; Quick et al., 2011; Valsecchi et al., 2013), 6 – Pakhuis Pass (Chase et al., 2019a; Scott and Woodborne, 2007a, 2007b), 7 – Elands Bay Cave (Cowling et al., 1999; Parkington et al., 2000), 8 – Pella (Chase et al., 2019b; Lim et al., 2016), 9 – Zizou (Chase et al., 2019b), 10 – Spitzkoppe (Chase et al., 2009, 2019b). (For interpretation of the references to colour in this figure legend, the reader is referred to the Web version of this article.)

Rickaby, 2009; Chase and Meadows, 2007; Cockcroft et al., 1987; Partridge et al., 1999; van Zinderen Bakker, 1976).

While this model maintains broad validity (Chase et al., 2017), and is still often applied, a growing body of evidence indicates that the response to changes in global boundary conditions between and within these rainfall zones has been more complex than previously supposed, with significant subregional variability observed in each of the summer (Burrough et al., 2009; Chase et al., 2019b, 2022; Chevalier and Chase, 2015), winter (Chase et al., 2015a, 2019a; Cowling et al., 1999; Parkington et al., 2000) and aseasonal (Chase et al., 2017; Chase and Quick, 2018; Scott et al., 2021) rainfall zones. In some cases, marked differences may occur across narrow spatial ranges, implying highly dynamic environmental gradients.

It has also been recognised in recent years, particularly in southwestern Africa, that aspects of these complexities can be considered not just in terms of moisture-bearing systems, but also in terms of those systems that inhibit precipitation or block moisture transport (Chase et al., 2015b). This was, in fact, recognised some time ago, with the establishment of the winter rainfall zone being associated with the global cooling during the Plio-Pleistocene and the associated intensification of the South Atlantic Anticyclone and Benguela Upwelling System (Etourneau et al., 2009; Tankard and Rogers, 1978). Driven by intra-hemispheric temperature gradients, increased coastal upwelling results from the establishment/intensification of a high-pressure cell along the coastal margin, which supresses local convection and blocks moisture-bearing systems from the tropics (Hou et al., 2020; Little et al., 1997; Sun et al., 2017). In southwestern Africa, (particularly the Cape region) reductions in summer rain may be compensated for by an increase in winter rainfall, as the westerly storm track is displaced equatorward. These factors are further considered to have accounted for the Pliocene shift from the subtropical woodlands and grasslands of the Miocene to the sclerophyllous Mediterranean shrublands that characterise the southwestern Cape today (Coetzee and Rogers, 1982; Dupont et al., 2011; Hendey, 1973; van Zinderen Bakker, 1975).

The impact of this dynamic is also evident during the glacial-interglacial cycles of the late Quaternary. Records from the Namib Desert, show that the Benguela system strongly influences climate, with a negative relationship between upwelling intensity and terrestrial humidity at centennial to multi-millennial timescales (Chase et al., 2023; Chase et al., 2010; Chase et al., 2009; Chase et al., 2019b). This blocking of tropical systems has been implicated as a driver of environmental change in the summer rainfall as far east as the Makgadikgadi basin of northern Botswana (Stokes et al., 1997), as well as in some records from the winter rainfall zone, where even modest contributions of summer rainfall may have had a significant impact on rainfall and drought season length/intensity (Chase et al., 2015a, 2015b). While this dynamic is recognised as a fundamental aspect of the WRZ climate system, and has been discussed at length in recent decades there are currently no continuous palaeoclimatic records that reliably reflect winter rainfall zone terrestrial climate variability across the marine isotope (MIS) 1–4 timeframe.

Addressing this need, this paper presents stable nitrogen isotope data from a WRZ rock hyrax midden, collected from the Groenfontein Private Nature Reserve in the Swartruggens Mountains. Extending from 1600 cal yr BP to an estimated 70,000 cal yr BP, the record provides a unique long-term perspective on local/sub-regional hydroclimates across MIS 1–4, with MIS 2–4 being particularly well-resolved. This record is significantly longer than those previously available from the region (~19,000 cal yrs BP from De Rif (Chase et al., 2015a; Chase et al., 2011) and ~23,000 cal yrs BP from Pakhuis Pass (Chase et al., 2019a; Scott and Woodborne, 2007b)), providing new insights into WRZ palaeoclimate during this period. These data also enable a more complete assessment of inter-regional climate dynamics during the last glacial period through comparison with the longer records available from the SRZ (Partridge et al., 1997) and ARZ (Chase et al., 2021).

1.1. Site description

This study details results from a 41.4 cm thick rock hyrax midden collected from a cliff (32.834°S, 19.532°E; 970 m. a.s.l.) in the sandstone tablelands of the Swartruggens mountains, a southeastern subsidiary range of the of the Cederberg Mountains, which form the dominant north-south axis of the Cape Fold Mountains in the region. As a whole, these mountains form an important divide between the Atlantic Ocean and winter-rain dominated southwestern Cape and the more arid western Karoo (Figs. 1 and 2). With the dominant atmospheric flow coming from the west, the Swartruggens range lies in the rainshadow of the (~2000 m) Skurweberge range 15 km to the west. Mean annual rainfall at the site is ~250 mm/yr, ~75% of which falls in the austral winter between May and September (Hijmans et al., 2005).

2. Material and methods

The Groenfontein-1 midden (Fig. 3) was selected for its thickness and high hyraceum (crystallised urine) content. Proxies obtained from hyraceum are considered to represent environmental conditions more clearly than samples containing high proportions of faecal pellets, which may 1) include a degree of dietary bias, 2) lack the stratigraphic integrity of hyraceum middens, and 3) are poor temporal integrators,

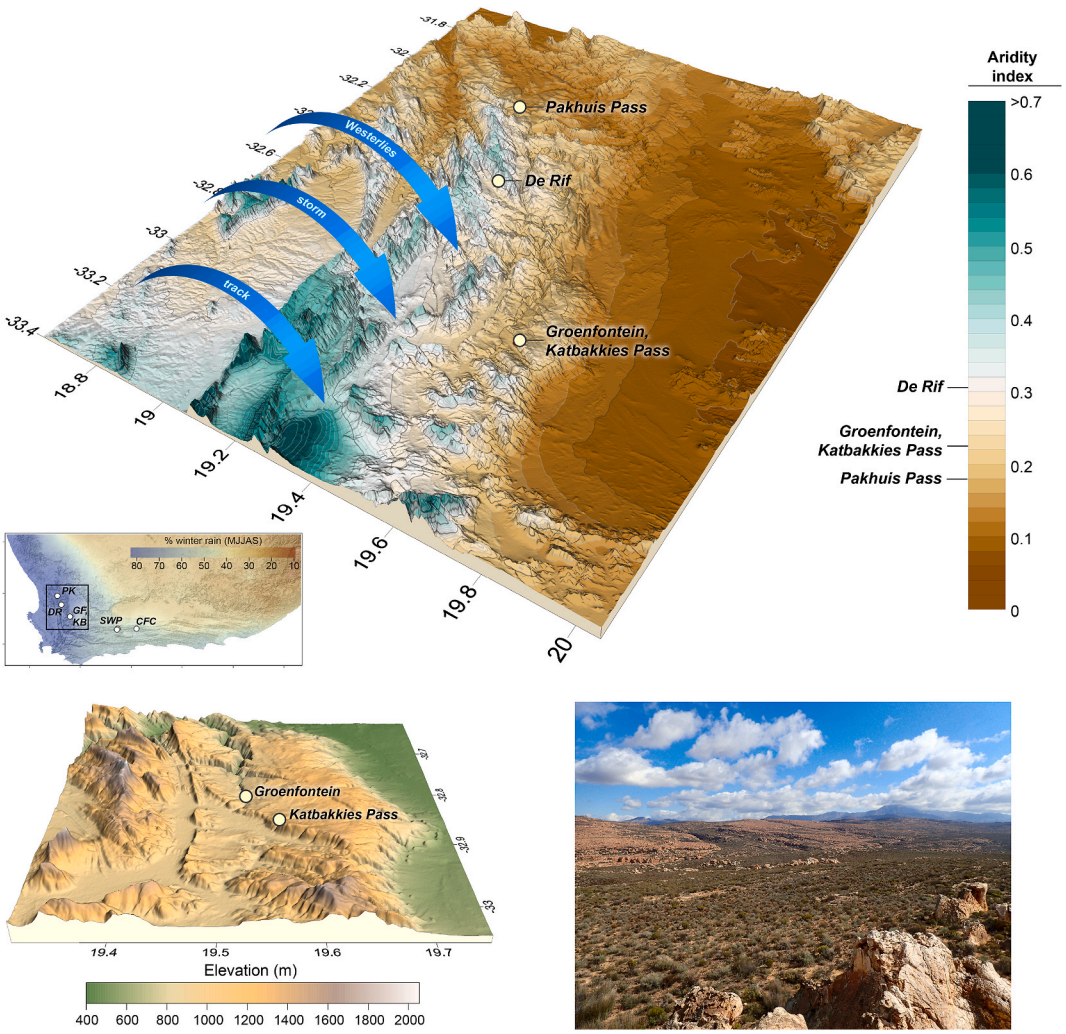

Fig. 2. Map of the N–S axis of the Cape Fold Mountains in the southwestern Cape, including the Cederberg Mountains and adjacent ranges. Topography is overlain by a map of mean Aridity Index values (Trabucco and Zomer, 2019), as in Fig. 1. The dominant vector of temperate moisture-bearing systems related to the westerly storm track is shown, as are the Groenfontein rock hyrax midden site (this study) and the other regional sites considered: Pakhuis Pass (Chase et al., 2019a; Scott and Woodborne, 2007a, 2007b), De Rif (Chase et al., 2011, 2015a; Quick et al., 2011) and Katbakkies Pass (Chase et al., 2015b; Meadows et al., 2010). The relative aridity of each site is shown on the legend. Inset indicates position of the region within the southwestern Cape (SWP = Seweweekspoort (Chase et al., 2013; Chase et al., 2017); CFC = Cape Fold speleothem composite (Chase et al., 2021)). Lower panes show the position of the Groenfontein site relative to the adjacent Katbakkies Pass site and show a view from the site across the plateau to the west of the site.

Fig. 3. The Groenfontein-1 rock hyrax midden, (A) in-situ (16 cm GPS unit for scale) and (B) with GF-1 section removed. (C) GF-1 section (rotated counter-clockwise 90°) with position of radiocarbon and stable isotope samples taken perpendicular to the accumulation axis indicated respectively by larger and smaller white dots.

reflecting the discrete periods during which the animals are consuming the food that is excreted as pellets (Chase et al., 2012). A representative section of the midden (Fig. 3) was cut perpendicular to the stratigraphy using an angle grinder and transported back to the laboratory for analysis. In the lab, the section was cleaned using progressively finer grades of sandpaper prior to sub-sampling.

2.1. Chronology

Radiocarbon age determinations for the GF-1 midden (n = 20) were processed at the ^{14}CHRONO Centre, Queen's University Belfast using accelerator mass spectrometry (AMS) (Table 1; Fig. 4). Samples were pre-treated with 2% HCl for one hour at room temperature to remove

Table 1
Radiocarbon ages and calibration information for the Groenfontein-1 rock hyrax midden.

Sample	Depth (mm)	14C age yr BP	1 sigma error	calibration data	95.4% (2σ) cal age ranges	95.4% (2σ) cal age ranges	relative area under distribution	median probability (cal BP)
					lower cal range BP	upper cal range BP		
UBA-32135	8.32	1158	26	SHCal20	959	−40.65	100.0%	1013
UBA-32137	9.77	1461	17	SHCal20	1293	1320	20.1%	1313
					1326	1353		
UBA-32089	41.76	4409	25	SHCal20	4855	4993	95.6%	4933
					4998	2041		
UBA-32140	49.62	11,831	30	SHCal20	13,517	13,547	100.0%	13,663
					13,585	13,762		
UBA-32141	59.81	13,155	36	SHCal20	15,583	15,891	100.0%	15,731
UBA-32142	70.19	14,227	37	SHCal20	17,088	17,381	100.0%	17,233
UBA-32090	79.39	14,726	66	SHCal20	17,814	18,205	100.0%	18,020
UBA-32143	91.76	16,261	65	SHCal20	19,437	19,832	100.0%	19,572
UBA-32144	108.13	17,170	70	SHCal20	20,512	20,867	100.0%	20,689
UBA-32091	125.11	20,072	80	SHCal20	23,845	24,238	100.0%	24,037
UBA-32145	138.02	23,915	134	SHCal20	27,739	28,424	100.0%	28,008
UBA-32146	148.93	26,026	172	SHCal20	29,987	30,739	100.0%	30,237
UBA32138	157.60	27,102	218	SHCal20	30,913	31,579	100.0%	31,167
UBA-32099	190.69	31,631	263	SHCal20	35,376	36,384	100.0%	35,925
UBA-32147	202.63	33,555	402	SHCal20	37,139	39,374	100.0%	38,341
UBA-32100	219.08	41,265	754	SHCal20	41,171	42,225	100.0%	41,740
UBA-32101	249.01	37,001	446	SHCal20	42,944	45,170	100.0%	44,099
UBA32139	278.78	46,813	3181	SHCal20	44,876	54,980	100.0%	49,596
UBA-32148	308.82	46,387	2110	SHCal20	45,240	52,793	92.1%	49,183
					53,430	54,980	0.1%	
UBA-32136	403.66	50,767	4320	SHCal20	N/A	N/A	N/A	N/A

carbonates and dried at 60 °C. They were then weighed into quartz tubes with an excess of CuO, sealed under vacuum and combusted to CO_2. The CO_2 was converted to graphite on an iron catalyst using the zinc reduction method (Slota et al., 1987). The dried samples were weighed in pre-purified tin capsules and burned in oxygen with helium carrier gas in the element analyzer (Elementar Vario Isotope), then transferred to the IonPlus AGE3 automated graphitization system, which uses the hydrogen reduction method (Němec et al., 2016). The radiocarbon ages were corrected for isotope fractionation using the AMS measured $\delta^{13}C$. The ages were calibrated using the SHCal20 calibration data (Hogg et al., 2020). The rbacon v.2.5.8 software package (Blaauw and Christen, 2011; Blaauw et al., 2020) was used to generate the age-depth model (Fig. 4).

2.2. Stable nitrogen isotopes

The stable nitrogen isotope composition of 374 hyraceum samples (approx. 2 mg) were measured at the School of Geography, Geology and the Environment, University of Leicester. Samples were obtained from two offset tracks using a 1 mm drill, creating a quasi-continuous record of overlapping samples (Fig. 3). Isotope ratios were measured on a Sercon 20-20 continuous flow isotope ratio mass spectrometer. For the stable isotope analyses, the standard deviation derived from replicate analyses of homogeneous reference material (Casein protein CatNo. B2155 Batch no. 114859 Elemental Microanalysis Ltd UK) was better than 0.2‰. The results are expressed relative to atmospheric nitrogen.

3. Results and interpretive basis

3.1. Chronology

Radiocarbon analyses indicate that the Groenfontein-1 hyrax midden likely accumulated during the last ~70,000 years (Table 1; Fig. 4). Analysis of hyraceum samples from the lower portions of the midden indicate that accumulation extends beyond the range of radiocarbon calibration. Using the mean ~150 yr/mm accumulation rate of the Pleistocene portion of the sequence, we have extrapolated the age model to provide an estimated chronological constraint for the lower portion of the midden. Considering this, the estimated age of samples predating what we deem to be the last reliable full calibration (44,876–54,980 cal BP at 278.78 mm) should be considered as speculative (Table 1; Fig. 5). The age-depth model for the Groenfontein-1 midden suggests continuous deposition, although accumulation rates during the early to mid-Holocene decrease dramatically (~1 mm/1110 years from ~4900 to 13700 cal BP).

3.2. Stable nitrogen isotopes and their interpretation

The $\delta^{15}N$ values from the Groenfontein-1 midden vary from −2.6 to 9.9‰. Continuous wavelet transform of the record indicates a significant influence of precessional forcing (19–23 kyr period) during the last glacial period and a transition to the dominance of suborbital factors at the end of MIS 2 (Fig. 5).

Variations in midden $\delta^{15}N$ are interpreted (as per other studies of nitrogen isotopes in hyraceum, e.g. Chase et al., 2019a; Chase et al., 2009; Chase et al., 2019b; Chase et al., 2012) to reflect changes in water availability. This is considered to be a function of a more open nitrogen cycle in arid regions, meaning that nitrogen in such regions is more prone to loss through transformation and the release of gaseous products is depleted in ^{15}N, and the remaining nitrogen in the soil is enriched (Austin and Vitousek, 1998). The $\delta^{15}N$ value of soils is thus higher with increasing aridity, and this is transmitted to, and replicated in, plant and animal tissues, including herbivore faecal matter (e.g. Aranibar et al., 2008; Carr et al., 2022; Carr et al., 2016; Craine et al., 2009; Handley et al., 1999; Hartman, 2011; Hartman and Danin, 2010; Murphy and Bowman, 2006, 2009; Newsome et al., 2011; Swap et al., 2004). Studies of ^{15}N in hyrax middens from a wide range of environments indicate consistently strong correlations between midden ^{15}N and independent climate proxy records, supporting the conclusion that environmental moisture availability is a major driver of midden ^{15}N records (Carr et al., 2016; Chase et al., 2009, 2015a, 2017, 2019b). Accordingly, we observe the most humid phases of the last 70 kyr occurred at approximately 54–58 ka and 29.4–37.3 cal ka BP, and (more tentatively given the loss of temporal resolution) during the mid-Holocene, with a shift to the most arid phase of the record occurring after the end of MIS 2 in the early Holocene.

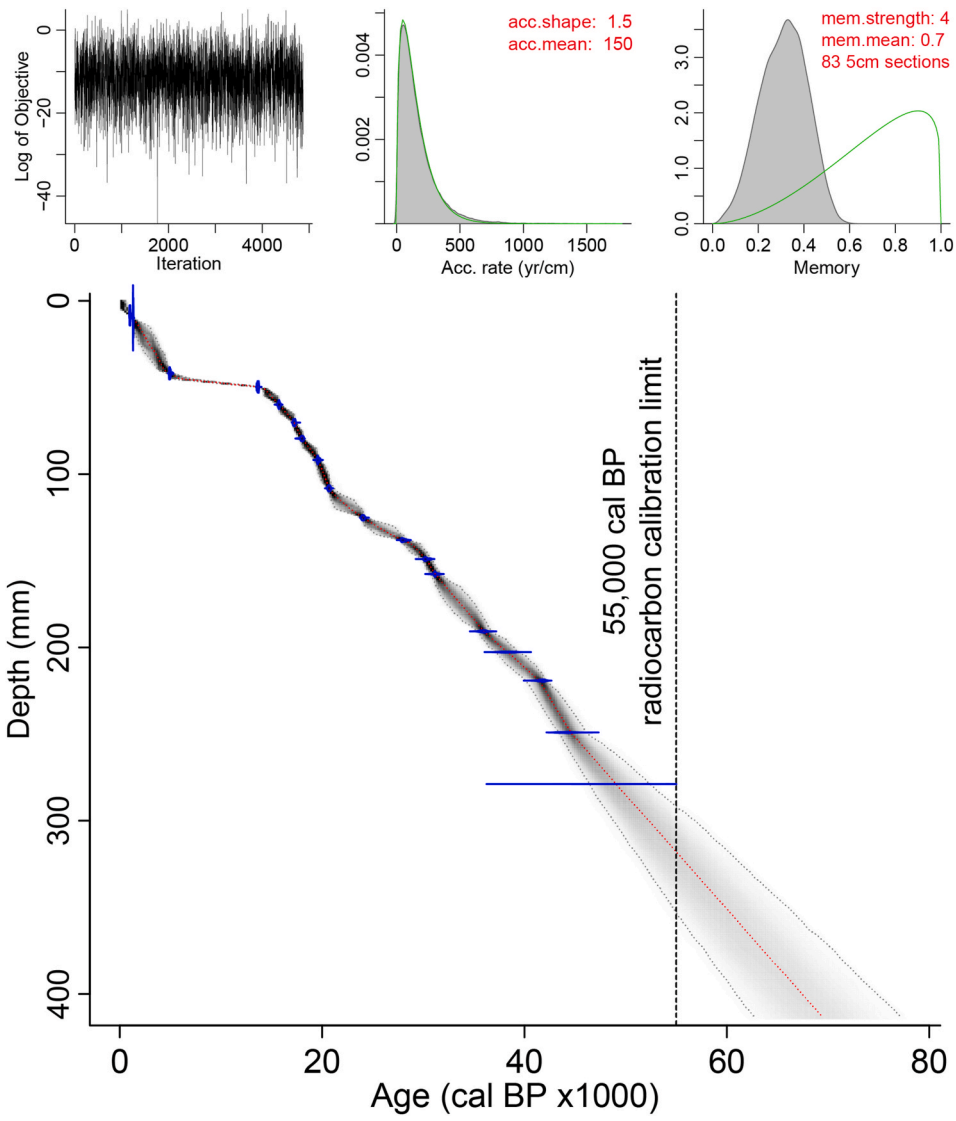

Fig. 4. Distribution in time and depth of ^{14}C ages for the Groenfontein-1 rock hyrax midden with age-depth model (grey), overlaying the calibrated distributions of the individual dates calculated using Bacon v2.5.8 (Blaauw and Christen, 2011). Red dotted lines indicate the 'best' model based on the mean age. Grey dotted lines indicate the 95% confidence ranges, and the greyscales describe the entire age model, with darker grey reflecting more likely ages. Samples from 308.8 mm to 403.6 mm were beyond the range of radiocarbon dating were not used for the calculation of the age-depth model and are not shown. (For interpretation of the references to colour in this figure legend, the reader is referred to the Web version of this article.)

4. Discussion

The Groenfontein-1 δ^{15}N record presented here is the longest continuous terrestrial record yet recovered from the WRZ. While constraints do exist on the inferences that can be drawn, given that: 1) midden accumulation extends beyond the range of radiocarbon calibration and 2) markedly lower accumulation rates are evident during the early Holocene, this record provides unique insight into WRZ climates during a large proportion of the last glacial period.

The estimated onset of midden accumulation near the beginning of MIS 4 and the sharp decrease in accumulation rate at the end of MIS 2 (Fig. 4) are broadly consistent with what can be considered glacial-age conditions, as reflected in the Cape Fold composite δ^{13}C record (Chase et al., 2021; including data from Braun et al., 2020; Chase et al., 2017; Talma and Vogel, 1992) (Fig. 6). This similarity in timing of midden accumulation may itself indicate changing climate conditions, with lower temperatures resulting in more effective rainfall (ΔP:PET) (Chevalier and Chase, 2016) and/or an increase in regional rainfall as the Subtropical Front and westerly storm track migrated equatorward (Bard and Rickaby, 2009).

During the last glacial period, from 70 ka through Heinrich stadial 1 (HS1; ~18–14.6 ka), phases of wetter and drier conditions at Groenfontein are consistent with orbital forcing associated with precessional cycles (Fig. 6). That the Groenfontein record maintains a consistent relationship with this parameter throughout the last glacial period (Fig. 7) provides support for the reliability of the extrapolated age model pre-dating ~50 cal ka BP. The relationship of the Groenfontein record with insolation, however, is not what may be predicted according to models of either direct precessional forcing (increased summer rainfall under higher austral summer insolation) or increased winter rainfall during periods of more extensive Antarctic sea-ice (concurrent with lower boreal summer insolation and global temperatures during the last glacial cycle) (Figs. 6 and 7). Rather, more humid conditions at Groenfontein during the last glacial period tend to conform to phases of high (low) boreal (austral) insolation. This does not negate the possibility, or indeed likelihood, that an equatorward migration of the Subtropical Front and westerly storm track resulted in an increase in winter rainfall in the southwestern Cape during the last glacial period (Chase et al., 2019a; Chase et al., 2017; Cockcroft et al., 1987; van Zinderen Bakker, 1976), but it does demand further consideration of the factors that determined the climate variability within this period. As described by Chase et al. (2015a, 2017), the variability observed in regional records may not relate only to changes in the dominant precipitation regime, but also to variations in dry-season precipitation, in this case summer rainfall associated with tropical easterly flow.

Acknowledging again that the chronology of the record that pre-

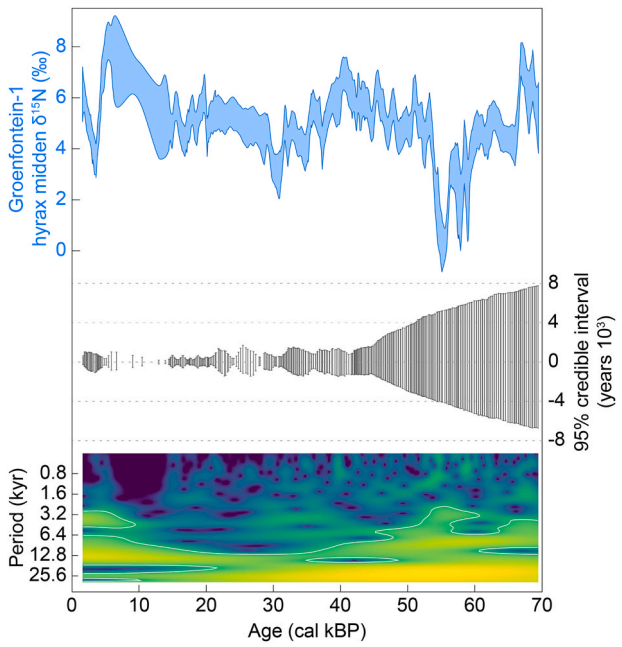

Fig. 5. The $\delta^{15}N$ data from the Groenfontein-1 rock hyrax midden. 95% credible interval associated with the age-depth model for each sample are indicated. Lower pane shows local Morlet wavelet power spectrum (higher (lower) signal power is shown in yellow (blue)) for the $\delta^{15}N$ record, with white line delimiting greater than 95% confidence using a white-noise model (Hammer et al., 2001). (For interpretation of the references to colour in this figure legend, the reader is referred to the Web version of this article.)

dates ~55 cal ka BP can only be tentatively constrained, similarities are apparent between the Groenfontein record and precipitation variability in the SRZ, which can be related to factors that limit the transport of tropical moisture into the southwestern Cape. As has been described elsewhere (Chase, 2021; Chase et al., 2021; Partridge et al., 1997; Simon et al., 2015), the relationship between precipitation in the eastern SRZ and summer insolation was strong under periods of high orbital eccentricity, but as eccentricity declined across the last glacial period this relationship broke down, particularly after ~70 ka, when Northern Hemisphere forcing appears to have become a dominant influence in the region (Chase et al., 2021; Chevalier and Chase, 2015). Comparison of the Groenfontein $\delta^{15}N$ record with the rainfall reconstruction from Tswaing Crater (Partridge et al., 1997) highlights an aspect of this regime shift, with an increasingly strong negative correlation between $\delta^{15}N$ at Groenfontein (lower values occur under wetter conditions) and rainfall at Tswaing Crater (Fig. 7). A direct influence of expanded tropical easterly flow could be inferred from this relationship, resulting in more summer rain at Groenfontein, and a shorter/less intense dry season. This may be supported by speleothem $\delta^{13}C$ data from the Cango Caves region of the southern Cape, with higher $\delta^{13}C$ values at 30.5 ka and 55 ka perhaps reflecting increases in warm growing season C_4 grasses at times of increased humidity at Groenfontein.

However, factors associated with climate variability at Groenfontein may not simply relate to changes in the strength of moisture-bearing systems, but also to those aspects of the regional climate system that determine their position and extent. From geologic to centennial timescales, the existence and dynamics of the WRZ have been shown to be intrinsically associated with coastal upwelling in the Benguela system, with global cooling intensifying the strength of the South Atlantic Anticyclone and the upwelling of cold water along the coast (Etourneau et al., 2009; Farmer et al., 2005; Little et al., 1997), effectively blocking the incursion of tropical moisture into the region (Chase et al., 2015a; Chase et al., 2015b; Coetzee and Rogers, 1982; Hendey, 1973; van Zinderen Bakker, 1975). This is highlighted in records obtained from

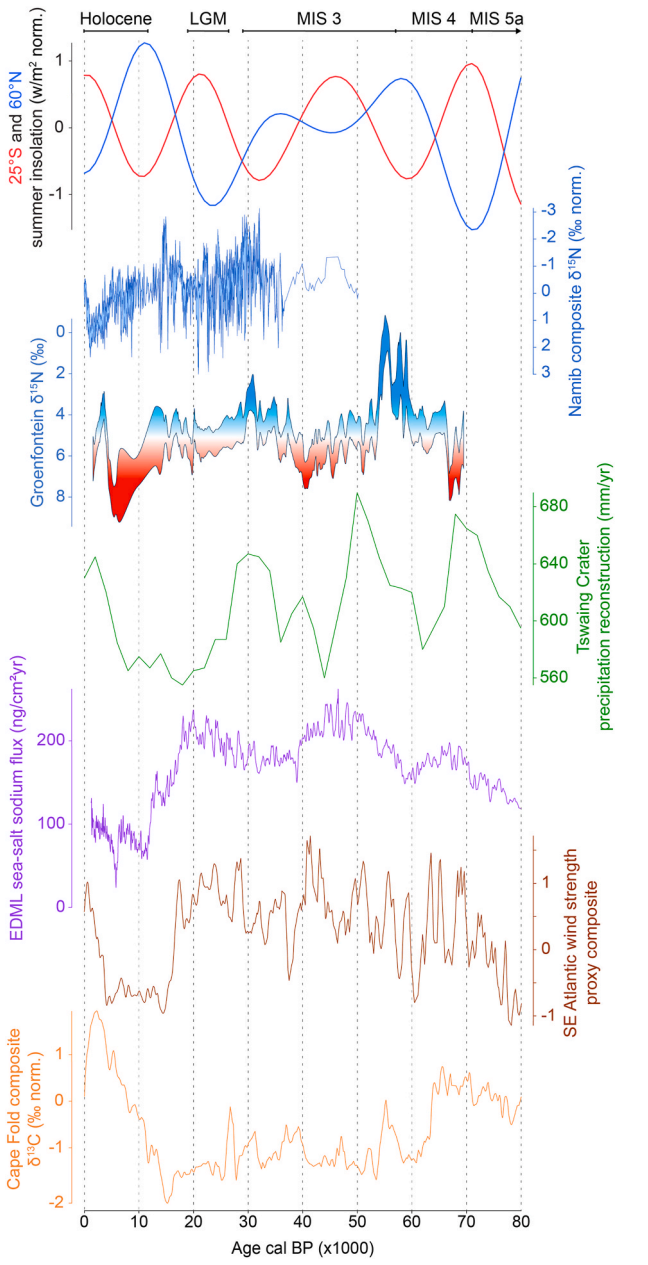

Fig. 6. Comparison of the $\delta^{15}N$ data from the Groenfontein-1 rock hyrax midden (shading: blue (red) = wetter (drier) than average conditions) with: summer insolation at 25°S and 60°N (Laskar et al., 2004), a composite $\delta^{15}N$ record from the Namib Desert region (Chase et al., 2019b), the precipitation reconstruction from Tswaing Crater (Partridge et al., 1997), the sea-salt sodium flux record from the Dronning Maud Land (EDML) Antarctic ice core (Fischer et al., 2007), a composite record of SE Atlantic wind strength proxies (higher values indicate increased wind strength; Chase et al., 2019a; data from Farmer et al., 2005; Little et al., 1997; Pichevin et al., 2005; Stuut et al., 2002), and the Cape Fold composite $\delta^{13}C$ record (Chase et al., 2021; including data from Braun et al., 2020; Chase et al., 2017; Talma and Vogel, 1992). (For interpretation of the references to colour in this figure legend, the reader is referred to the Web version of this article.)

hyrax middens from De Rif, in the Cederberg (Figs. 1 and 2), where similarities between hyraceum $\delta^{15}N$ and sea-surface temperature reconstructions suggest a strong negative relationship between humidity at De Rif and coastal upwelling (Chase et al., 2011, 2015a). To the north, hyrax midden records from the Namib Desert region of the western SRZ also indicate a negative relationship between humidity and upwelling, most notably at orbital timescales, with phases of wetter conditions

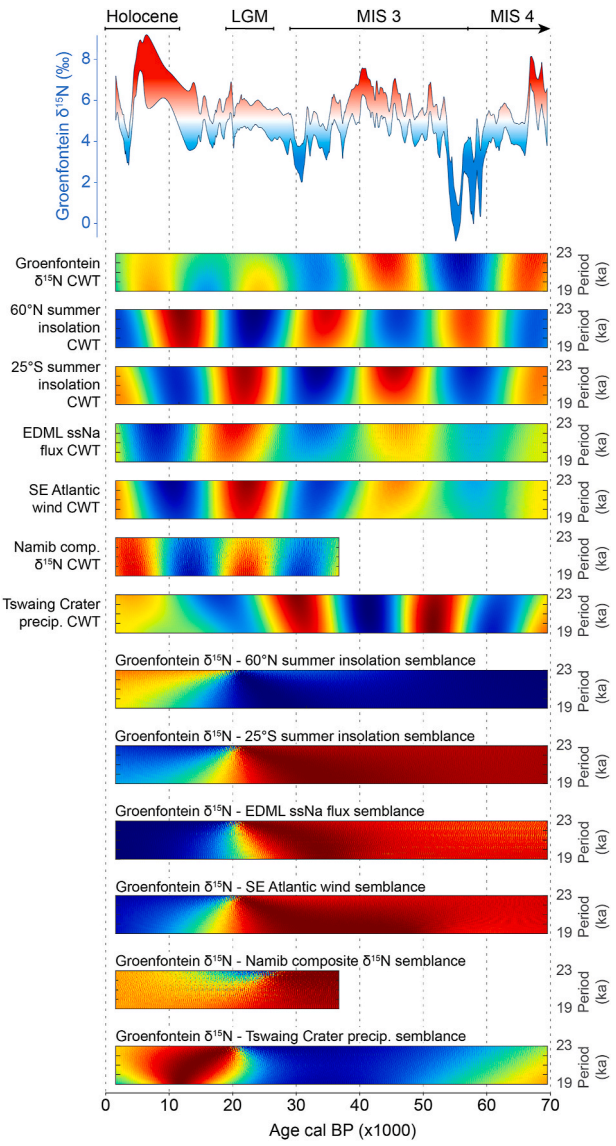

Fig. 7. Comparison of real-value wavelet power spectra at 19-23-kyr periods from continuous Morlet wavelet transforms of: 1) the Groenfontein $\delta^{15}N$ record (this paper), 2) summer insolation at 60°N and 25°S (Laskar et al., 2004), 3) the sea-salt sodium flux record from the Dronning Maud Land (EDML) Antarctic ice core (Fischer et al., 2007), 4) a composite record of SE Atlantic wind strength proxies (higher values indicate increased wind strength; Chase et al., 2019a; data from Farmer et al., 2005; Little et al., 1997; Pichevin et al., 2005; Stuut et al., 2002), 5) a composite $\delta^{15}N$ record from the Namib Desert region (Chase et al., 2019b), and 6) the precipitation reconstruction from Tswaing Crater (Partridge et al., 1997). The colour gradient indicates real-value wavelet power (red indicates large positive anomalies while blue indicates large negative anomalies). The relationship between the Groenfontein $\delta^{15}N$ record and these regional, remote and external records is assessed using wavelet-based semblance analysis (Cooper and Cowan, 2008). In the semblance diagrams, red indicates a semblance of +1 (positive correlation), and blue indicates a semblance of −1 (negative correlation). (For interpretation of the references to colour in this figure legend, the reader is referred to the Web version of this article.)

being associated with increased summer insolation at 60°N and decreased summer insolation at 25°S (Chase et al., 2019b). Conditions at Groenfontein appear to be controlled by this same dynamic during the last glacial period. The well-resolved portions of the Groenfontein and Namib Desert hyrax middens (37–12.6 cal ka BP) show clear similarities at precessional (19–23 kyr) periods (Figs. 5–7), consistent with decreased summer insolation at 60°N resulting in cooler global temperatures, increased intra-hemispheric temperature gradients and South Atlantic Anticyclone intensity, and more effective blocking of tropical easterly moisture flow.

At suborbital timescales, the impact of the iceberg rafting and freshening of the North Atlantic Basin associated with HS1 (~18–14.6 cal ka BP) has been identified at many sites in southwestern Africa, generally with elevated sea-surface temperatures and increased tropical/summer rainfall resulting in wetter conditions (Chase et al., 2015a, 2019a; Quick et al., 2021). At Groenfontein, this period marks a transition between glacial and interglacial boundary conditions and regional climate regimes. While the post-HS1 portion of the Groenfontein $\delta^{15}N$ record is less well-resolved, it does indicate that the strong glacial-age influence of high northern latitude insolation and associated changes in Benguela upwelling breaks down (Figs. 6 and 7), and there appears to be a fundamental shift in the influence of circulation systems in the region. Records from nearby Pakhuis Pass (Chase et al., 2019a) and further afield to the east at Seweweekspoort (Fig. 2; Chase et al., 2017) indicate a progressive decline in water availability from the LGM into the Holocene, consistent with models suggesting a decrease in winter rainfall at this time (Cockcroft et al., 1987; van Zinderen Bakker, 1976). At Groenfontein, it seems likely that this reduction in winter rainfall resulted in more arid conditions at the site, despite a coeval reduction in coastal upwelling intensity (Fig. 6). Considering data from Seweekspoort, it has been proposed that centennial to millennial scale climate variability has been primarily determined by changes in the non-dominant moisture-bearing system (in this case the westerlies, under the warmer conditions and increased convective potential of the Holocene) (Chase et al., 2017). Other sites in the lee of the N–S axis of the Cape Fold mountains (Pakhuis Pass (Chase et al., 2019a) and Katbakkies Pass (Chase et al., 2015b; Meadows et al., 2010)) have preserved better-resolved Holocene sequences that have been associated with changes in the position of the westerlies. The mid-/late Holocene peak in humidity in the Groenfontein record is not – considered broadly – inconsistent with these findings, and the proximity of the Katbakkies Pass site (7.3 km to the south) would suggest that the two sites experienced similar environmental histories. However, the complexity of the region's response to changes in climate drivers (see Chase et al., 2019a) indicate that more detailed Holocene records are required before more definitive inferences can be drawn.

5. Conclusions

The data presented in this paper suggest climate variability in the South African winter rainfall zone is controlled by the position of the mid-latitude storm track and the strength of coastal upwelling, which modulates the incursion of moisture via the tropical easterlies. The timing of onset of midden accumulation and the evidence for relatively humid conditions during the last glacial period suggest that an equatorward displacement of the southern westerlies and associated frontal systems was fundamental in bringing increased moisture to the region at this time. However, a key new insight from this record is that in addition, climate variability during the last glacial period is characterised by a clear precessional signal that is inconsistent with changes in sea-ice extent, the putative driver of the position and influence of the mid-latitude storm track. Rather, a strong relationship with coastal upwelling in the Benguela system is identified, suggesting that the blocking of tropical easterlies flow may have been the primary driver of climate variability during this time, via its impact on the duration/intensity of the dry seasons. This is actually consistent with the mechanisms that over geological timescales led to the establishment of the winter rainfall zone and its mediterranean ecosystems. The marked aridification at the site after MIS 2 is similar to that observed at other sites in the rainshadow of this N–S axis of the Cape Fold mountains, and is interpreted as indicating a poleward shift of the mid-latitude storm track and a reduction in winter rainfall. The lower accumulation rate of the

Holocene portion of the record limits its potential for reliable inter-site comparison, and the observed spatial patterning of hydroclimate anomalies in southern Africa requires further resolution, but these data provide critical insight into the long-term drivers of environmental change in the southern African winter rainfall zone. It is also apparent that the Groenfontein rock hyrax midden represents a thus far unique terrestrial paleoenvironmental and (potential) palaeoecological archive for the winter rainfall zone and the Cape Floristic Region. Future work will seek to integrate the climatic record presented here with palaecological proxies from this midden, particularly to consider long-standing questions surrounding the response(s) of the hyper-diverse Fynbos Biome to Pleistocene climatic variability.

Declaration of competing interest

The authors declare that they have no known competing financial interests or personal relationships that could have appeared to influence the work reported in this paper.

Acknowledgements

The research leading to these results has received funding from the European Research Council under the European Union's Seventh Framework Programme (FP7/2007–2013), ERC Starting Grant "HYRAX", grant agreement no. 258657. The authors would like to thank Nicholas Wilshire for contacting us regarding the hyrax midden analysed for this study and Volker Miros and the owners of the Groenfontein Private Nature Reserve for allowing us to access to their land to collect midden material.

References

Aranibar, J.N., Anderson, I.C., Epstein, H.E., Feral, C.J.W., Swap, R.J., Ramontsho, J., Macko, S.A., 2008. Nitrogen isotope composition of soils, C_3 and C_4 plants along land use gradients in southern Africa. J. Arid Environ. 72, 326–337.

Austin, A.T., Vitousek, P.M., 1998. Nutrient dynamics on a precipitation gradient in Hawai'i. Oecologia 113, 519–529.

Bard, E., Rickaby, R.E.M., 2009. Migration of the subtropical front as a modulator of glacial climate. Nature 460, 380–383.

Blaauw, M., Christen, J.A., 2011. Flexible paleoclimate age-depth models using an autoregressive gamma process. Bayesian Analysis 6, 457–474.

Blaauw, M., Christen, J.A., L., A, A.M., 2020. Rbacon: Age-Depth Modelling Using Bayesian Statistics. R package version 2.5.6.

Braun, K., Bar-Matthews, M., Matthews, A., Ayalon, A., Zilberman, T., Cowling, R.M., Fisher, E.C., Herries, A.I.R., Brink, J.S., Marean, C.W., 2020. Comparison of climate and environment on the edge of the palaeo-agulhas plain to the Little Karoo (South Africa) in marine isotope stages 5–3 as indicated by speleothems. Quat. Sci. Rev. 235, 105803.

Burrough, S.L., Thomas, D.S.G., Singarayer, J.S., 2009. Late Quaternary hydrological dynamics in the Middle Kalahari: forcing and feedbacks. Earth Sci. Rev. 96, 313–326.

Carr, A.S., Chase, B.M., Boom, A., Meadows, M.E., Sanchez, J.M., 2022. Variability in soil and foliar stable carbon and nitrogen isotope compositions in the winter rainfall biomes of South Africa. J. Arid Environ. 200, 104726.

Carr, A.S., Chase, B.M., Boom, A., Medina-Sanchez, J., 2016. Stable isotope analyses of rock hyrax faecal pellets, hyraceum and associated vegetation in southern Africa: implications for dietary ecology and palaeoenvironmental reconstructions. J. Arid Environ. 134, 33–48.

Chase, B.M., 2021. Orbital forcing in southern Africa: towards a conceptual model for predicting deep time environmental change from an incomplete proxy record. Quat. Sci. Rev. 265, 107050.

Chase, B.M., Boom, A., Carr, A.S., Carré, M., Chevalier, M., Meadows, M.E., Pedro, J.B., Stager, J.C., Reimer, P.J., 2015a. Evolving southwest African response to abrupt deglacial North Atlantic climate change events. Quat. Sci. Rev. 121, 132–136.

Chase, B.M., Boom, A., Carr, A.S., Chevalier, M., Quick, L.J., Verboom, G.A., Reimer, P. J., 2019a. Extreme hydroclimate response gradients within the western Cape floristic region of South Africa since the last glacial maximum. Quat. Sci. Rev. 219, 297–307.

Chase, B.M., Boom, A., Carr, A.S., Meadows, M.E., Lim, S., (2023). A ~39,000-year record of vegetation and climate change from the margin of the Namib Sand Sea. Quat. Res..

Chase, B.M., Boom, A., Carr, A.S., Meadows, M.E., Reimer, P.J., 2013. Holocene climate change in southernmost South Africa: rock hyrax middens record shifts in the southern westerlies. Quat. Sci. Rev. 82, 199–205.

Chase, B.M., Boom, A., Carr, A.S., Reimer, P.J., 2022. Climate variability along the margin of the southern African monsoon region at the end of the African Humid Period. Quat. Sci. Rev. 291, 107663.

Chase, B.M., Chevalier, M., Boom, A., Carr, A.S., 2017. The dynamic relationship between temperate and tropical circulation systems across South Africa since the last glacial maximum. Quat. Sci. Rev. 174, 54–62.

Chase, B.M., Harris, C., de Wit, M.J., Kramers, J., Doel, S., Stankiewicz, J., 2021. South African Speleothems Reveal Influence of High- and Lowlatitude Forcing over the Past 113.5 k.Y. Geology.

Chase, B.M., Lim, S., Chevalier, M., Boom, A., Carr, A.S., Meadows, M.E., Reimer, P.J., 2015b. Influence of tropical easterlies in southern Africa's winter rainfall zone during the Holocene. Quat. Sci. Rev. 107, 138–148.

Chase, B.M., Meadows, M.E., 2007. Late Quaternary dynamics of southern Africa's winter rainfall zone. Earth Sci. Rev. 84, 103–138.

Chase, B.M., Meadows, M.E., Carr, A.S., Reimer, P.J., 2010. Evidence for progressive Holocene aridification in southern Africa recorded in Namibian hyrax middens: implications for African Monsoon dynamics and the "African Humid Period''. Quat. Res. 74, 36–45.

Chase, B.M., Meadows, M.E., Scott, L., Thomas, D.S.G., Marais, E., Sealy, J., Reimer, P.J., 2009. A record of rapid Holocene climate change preserved in hyrax middens from southwestern Africa. Geology 37, 703–706.

Chase, B.M., Niedermeyer, E.M., Boom, A., Carr, A.S., Chevalier, M., He, F., Meadows, M. E., Ogle, N., Reimer, P.J., 2019b. Orbital controls on Namib Desert hydroclimate over the past 50,000 years. Geology 47, 867–871.

Chase, B.M., Quick, L.J., 2018. Influence of Agulhas forcing of Holocene climate change in South Africa's southern Cape. Quat. Res. 90, 303–309.

Chase, B.M., Quick, L.J., Meadows, M.E., Scott, L., Thomas, D.S.G., Reimer, P.J., 2011. Late glacial interhemispheric climate dynamics revealed in South African hyrax middens. Geology 39, 19–22.

Chase, B.M., Scott, L., Meadows, M.E., Gil-Romera, G., Boom, A., Carr, A.S., Reimer, P.J., Truc, L., Valsecchi, V., Quick, L.J., 2012. Rock hyrax middens: a palaeoenvironmental archive for southern African drylands. Quat. Sci. Rev. 56, 107–125.

Chevalier, M., Chase, B.M., 2015. Southeast African records reveal a coherent shift from high- to low-latitude forcing mechanisms along the east African margin across last glacial–interglacial transition. Quat. Sci. Rev. 125, 117–130.

Chevalier, M., Chase, B.M., 2016. Determining the drivers of long-term aridity variability: a southern African case study. J. Quat. Sci. 31, 143–151.

Cockcroft, M.J., Wilkinson, M.J., Tyson, P.D., 1987. The application of a present-day climatic model to the late Quaternary in southern Africa. Climatic Change 10, 161–181.

Coetzee, J.A., Rogers, J., 1982. Palynological and lithological evidence for the Miocene palaeoenvironment in the Saldanha region (South Africa). Palaeogeogr. Palaeoclimatol. Palaeoecol. 39, 71–85.

Cooper, G.R.J., Cowan, D.R., 2008. Comparing time series using wavelet-based semblance analysis. Comput. Geosci. 34, 95–102.

Cowling, R.M., Cartwright, C.R., Parkington, J.E., Allsopp, J.C., 1999. Fossil wood charcoal assemblages from Elands Bay Cave, South Africa: implications for Late Quaternary vegetation and climates in the winter-rainfall fynbos biome. J. Biogeogr. 26, 367–378.

Craine, J.M., Elmore, A.J., Aidar, M.P.M., Bustamante, M., Dawson, T.E., Hobbie, E.A., Kahmen, A., Mack, M.C., McLauchlan, K.K., Michelsen, A., Nardoto, G.B., Pardo, L. H., Peñuelas, J., Reich, P.B., Schuur, E.A.G., Stock, W.D., Templer, P.H., Virginia, R. A., Welker, J.M., Wright, I.J., 2009. Global patterns of foliar nitrogen isotopes and their relationships with climate, mycorrhizal fungi, foliar nutrient concentrations, and nitrogen availability. New Phytol. 183, 980–992.

Crétat, J., Pohl, B., Dieppois, B., Berthou, S., Pergaud, J., 2019. The Angola Low: relationship with southern African rainfall and ENSO. Clim. Dynam. 52, 1783–1803.

Crétat, J., Richard, Y., Pohl, B., Rouault, M., Reason, C., Fauchereau, N., 2012. Recurrent daily rainfall patterns over South Africa and associated dynamics during the core of the austral summer. Int. J. Climatol. 32, 261–273.

Deacon, J., Lancaster, N., 1988. Late Quaternary Palaeoenvironments of Southern Africa. Clarendon Press, Oxford.

Dupont, L.M., Linder, H.P., Rommerskirchen, F., Schefuß, E., 2011. Climate-driven rampant speciation of the Cape flora. J. Biogeogr. 38, 1059–1068.

Etourneau, J., Martinez, P., Blanz, T., Schneider, R., 2009. Pliocene-Pleistocene variability of upwelling activity, productivity, and nutrient cycling in the Benguela region. Geology 37, 871–874.

Farmer, E.C., deMenocal, P.B., Marchitto, T.M., 2005. Holocene and deglacial ocean temperature variability in the Benguela upwelling region: implications for low-latitude atmospheric circulation. Paleoceanography 20. https://doi.org/10.1029/2004PA001049.

Fischer, H., Fundel, F., Ruth, U., Twarloh, B., Wegner, A., Udisti, R., Becagli, S., Castellano, E., Morganti, A., Severi, M., Wolff, E., Littot, G., Röthlisberger, R., Mulvaney, R., Hutterli, M.A., Kaufmann, P., Federer, U., Lambert, F., Bigler, M., Hansson, M., Jonsell, U., de Angelis, M., Boutron, C., Siggaard-Andersen, M.-L., Steffensen, J.P., Barbante, C., Gaspari, V., Gabrielli, P., Wagenbach, D., 2007. Reconstruction of millennial changes in dust emission, transport and regional sea ice coverage using the deep EPICA ice cores from the Atlantic and Indian Ocean sector of Antarctica. Earth Planet Sci. Lett. 260, 340–354.

Hammer, Ø., Harper, D.A.T., Ryan, P.D., 2001. PAST: paleontological statistics software package for education and data analysis. Palaeontol. Electron. 4, 9.

Handley, L.L., Austin, A.T., Stewart, G.R., Robinson, D., Scrimgeour, C.M., Raven, J.A., Heaton, T.H.E., Schmidt, S., 1999. The ^{15}N natural abundance ($\delta^{15}N$) of ecosystem samples reflects measures of water availability. Funct. Plant Biol. 26, 185–199.

Hartman, G., 2011. Are elevated $\delta^{15}N$ values in herbivores in hot and arid environments caused by diet or animal physiology? Funct. Ecol. 25, 122–131.

Hartman, G., Danin, A., 2010. Isotopic values of plants in relation to water availability in the Eastern Mediterranean region. Oecologia 162, 837–852.

Hendey, Q.B., 1973. Fossil occurrences at langebaanweg, Cape province. Nature 244, 13–14.
Hijmans, R., Cameron, S.E., Parra, J.L., Jones, P.G., Jarvis, A., 2005. Very high resolution interpolated climate surfaces for global land areas. Int. J. Climatol. 25, 1965–1978.
Hogg, A.G., Heaton, T.J., Hua, Q., Palmer, J.G., Turney, C.S.M., Southon, J., Bayliss, A., Blackwell, P.G., Boswijk, G., Bronk Ramsey, C., Pearson, C., Petchey, F., Reimer, P., Reimer, R., Wacker, L., 2020. SHCal20 southern Hemisphere calibration, 0–55,000 years cal BP. Radiocarbon 1–20.
Hou, A., Bahr, A., Schmidt, S., Strebl, C., Albuquerque, A.L., Chiessi, C.M., Friedrich, O., 2020. Forcing of western tropical South Atlantic sea surface temperature across three glacial-interglacial cycles. Global Planet. Change 188, 103150.
Laskar, J., Robutel, P., Joutel, F., Gastineau, M., Correia, A.C.M., Levrard, B., 2004. A long-term numerical solution for the insolation quantities of the Earth. A&A 428, 261–285.
Lim, S., Chase, B.M., Chevalier, M., Reimer, P.J., 2016. 50,000 years of vegetation and climate change in the southern Namib Desert, Pella, South Africa. Palaeogeogr. Palaeoclimatol. Palaeoecol. 451, 197–209.
Little, M.G., Schneider, R.R., Kroon, D., Price, B., Bickert, T., Wefer, G., 1997. Rapid palaeoceanographic changes in the Benguela Upwelling System for the last 160,000 years as indicated by abundances of planktonic foraminifera. Palaeogeogr. Palaeoclimatol. Palaeoecol. 130, 135–161.
Meadows, M.E., Chase, B.M., Seliane, M., 2010. Holocene palaeoenvironments of the Cederberg and Swartruggens mountains, Western Cape, South Africa: pollen and stable isotope evidence from hyrax dung middens. J. Arid Environ. 74, 786–793.
Murphy, B.P., Bowman, D.M.J.S., 2006. Kangaroo metabolism does not cause the relationship between bone collagen $\delta^{15}N$ and water availability. Funct. Ecol. 20, 1062–1069.
Murphy, B.P., Bowman, D.M.J.S., 2009. The carbon and nitrogen isotope composition of Australian grasses in relation to climate. Funct. Ecol. 23, 1040–1049.
Němec, M., Wacker, L., Gäggeler, H., 2016. Optimization of the graphitization process at age-1. Radiocarbon 52, 1380–1393.
Newsome, S.D., Miller, G.H., Magee, J.W., Fogel, M.L., 2011. Quaternary record of aridity and mean annual precipitation based on $\delta^{15}N$ in ratite and dromornithid eggshells from Lake Eyre, Australia. Oecologia 167, 1151–1162.
Parkington, J., Cartwright, C., Cowling, R.M., Baxter, A., Meadows, M., 2000. Palaeovegetation at the last glacial maximum in the western Cape, South Africa: wood charcoal and pollen evidence from Elands Bay Cave. South Afr. J. Sci. 96, 543–546.
Partridge, T.C., deMenocal, P.B., Lorentz, S.A., Paiker, M.J., Vogel, J.C., 1997. Orbital forcing of climate over South Africa: a 200,000-year rainfall record from the Pretoria Saltpan. Quat. Sci. Rev. 16, 1125–1133.
Partridge, T.C., Scott, L., Hamilton, J.E., 1999. Synthetic reconstructions of southern african environments during the last glacial maximum (21-18 kyr) and the Holocene altithermal (8-6 kyr). Quat. Int. 57–8, 207–214.
Pichevin, L., Cremer, M., Giraudeau, J., Bertrand, P., 2005. A 190 kyr record of lithogenic grain-size on the Namibian slope: forging a tight link between past wind-strength and coastal upwelling dynamics. Mar. Geol. 218, 81–96.
Quick, L.J., Chase, B.M., Carr, A.S., Chevalier, M., Grobler, B.A., Meadows, M.E., 2021. A 25,000 year record of climate and vegetation change from the southwestern Cape coast, South Africa. Quat. Res. 105, 82–99.
Quick, L.J., Chase, B.M., Meadows, M.E., Scott, L., Reimer, P.J., 2011. A 19.5 kyr vegetation history from the central Cederberg Mountains, South Africa: palynological evidence from rock hyrax middens. Palaeogeogr. Palaeoclimatol. Palaeoecol. 309, 253–270.
Reason, C.J.C., Rouault, M., Melice, J.L., Jagadheesha, D., 2002. Interannual winter rainfall variability in SW South Africa and large scale ocean–atmosphere interactions. Meteorol. Atmos. Phys. 80, 19–29.
Reynolds, R.W., Smith, T.M., Liu, C., Chelton, D.B., Casey, K.S., Schlax, M.G., 2007. Daily high-resolution-blended analyses for sea surface temperature. J. Clim. 20, 5473–5496.
Rouault, M., Florenchie, P., Fauchereau, N., Reason, C.J.C., 2003. South East tropical Atlantic warm events and southern African rainfall. Geophys. Res. Lett. 30.
Rouault, M., White, S.A., Reason, C.J.C., Lutjeharms, J.R.E., Jobard, I., 2002. Ocean–Atmosphere Interaction in the Agulhas Current Region and a South African Extreme Weather Event, vol. 17. Weather & Forecasting, p. 655.
Scott, L., Manzano, S., Carr, A.S., Cordova, C., Ochando, J., Bateman, M.D., Carrión, J.S., 2021. A 14000 year multi-proxy alluvial record of ecotone changes in a Fynbos-Succulent Karoo transition in South Africa. Palaeogeogr. Palaeoclimatol. Palaeoecol. 569, 110331.
Scott, L., Woodborne, S., 2007a. Pollen analysis and dating of late quaternary faecal deposits (hyraceum) in the Cederberg, western Cape, South Africa. Rev. Palaeobot. Palynol. 144, 123–134.
Scott, L., Woodborne, S., 2007b. Vegetation history inferred from pollen in Late Quaternary faecal deposits (hyraceum) in the Cape winter-rain region and its bearing on past climates in South Africa. Quat. Sci. Rev. 26, 941–953.
Simon, M.H., Ziegler, M., Bosmans, J., Barker, S., Reason, C.J.C., Hall, I.R., 2015. Eastern South African hydroclimate over the past 270,000 years. Sci. Rep. 5, 18153.
Slota, P.J., Jull, A.J.T., Linick, T.W., Toolin, L.J., 1987. Preparation of small samples for ^{14}C accelerator targets by catalytic reduction of CO. Radiocarbon 29, 303–306.
Stokes, S., Thomas, D.S.G., Washington, R., 1997. Multiple episodes of aridity in southern Africa since the last interglacial period. Nature 388, 154–158.
Stuut, J.-B.W., Prins, M.A., Schneider, R.R., Weltje, G.J., Jansen, J.H.F., Postma, G., 2002. A 300 kyr record of aridity and wind strength in southwestern Africa: inferences from grain-size distributions of sediments on Walvis Ridge, SE Atlantic. Mar. Geol. 180, 221–233.
Sun, X., Cook, K.H., Vizy, E.K., 2017. The South atlantic subtropical high: climatology and interannual variability. J. Clim. 30, 3279–3296.
Swap, R.J., Aranibar, J.N., Dowty, P.R., Gilhooly, W.P., Macko, S.A., 2004. Natural abundance of ^{13}C and ^{15}N in C_3 and C_4 vegetation of southern Africa: patterns and implications. Global Change Biol. 10, 350–358.
Talma, A.S., Vogel, J.C., 1992. Late quaternary paleotemperatures derived from a speleothem from Cango Caves, Cape province, South Africa. Quat. Res. 37, 203–213.
Tankard, A.J., Rogers, J., 1978. Late cenozoic palaeoenvironments on the west coast of southern Africa. J. Biogeogr. 5, 319–337.
Trabucco, A., Zomer, R., 2019. In: figshare (Ed.), Global Aridity Index and Potential Evapotranspiration (ET0) Climate Database V2.
Tyson, P.D., Cooper, G.R.J., McCarthy, T.S., 2002. Millennial to multi-decadal variability in the climate of southern Africa. Int. J. Climatol. 22, 1105–1117.
Valsecchi, V., Chase, B.M., Slingsby, J.A., Carr, A.S., Quick, L.J., Meadows, M.E., Cheddadi, R., Reimer, P.J., 2013. A high resolution 15,600-year pollen and microcharcoal record from the Cederberg Mountains, South Africa. Palaeogeogr. Palaeoclimatol. Palaeoecol. 387, 6–16.
van Zinderen Bakker, E.M., 1975. The origin and palaeoenvironment of the Namib Desert biome. J. Biogeogr. 2, 65–73.
van Zinderen Bakker, E.M., 1976. The evolution of late Quaternary paleoclimates of Southern Africa. Palaeoecol. Afr. 9, 160–202.